

## Experimental study on multi-channel waveform agile beamforming and testbed calibration

Ahmed, Sheeraz ; Aubry, Pascal ; Yarovoy, Alexander

**DOI**

[10.1109/CAMA49227.2021.9703587](https://doi.org/10.1109/CAMA49227.2021.9703587)

**Publication date**

2021

**Document Version**

Final published version

**Published in**

2021 IEEE Conference on Antenna Measurements & Applications (CAMA)

**Citation (APA)**

Ahmed, S., Aubry, P., & Yarovoy, A. (2021). Experimental study on multi-channel waveform agile beamforming and testbed calibration. In *2021 IEEE Conference on Antenna Measurements & Applications (CAMA): Proceedings* (pp. 248-253). Article 9703587 IEEE.  
<https://doi.org/10.1109/CAMA49227.2021.9703587>

**Important note**

To cite this publication, please use the final published version (if applicable).  
Please check the document version above.

**Copyright**

Other than for strictly personal use, it is not permitted to download, forward or distribute the text or part of it, without the consent of the author(s) and/or copyright holder(s), unless the work is under an open content license such as Creative Commons.

**Takedown policy**

Please contact us and provide details if you believe this document breaches copyrights.  
We will remove access to the work immediately and investigate your claim.

***Green Open Access added to TU Delft Institutional Repository***

***'You share, we take care!' - Taverne project***

**<https://www.openaccess.nl/en/you-share-we-take-care>**

Otherwise as indicated in the copyright section: the publisher is the copyright holder of this work and the author uses the Dutch legislation to make this work public.

# Experimental study on multi-channel waveform agile beamforming and testbed calibration

Sheeraz Ahmed, Pascal Aubry and Alexander Yarovoy

*Microwave Sensing, Signals and Systems (MS3)*

*Delft University of Technology*

Delft, The Netherlands

sheerazahmed021@outlook.com, {P.J.Aubry, A.Yarovoy} @tudelft.nl

**Abstract**—In this paper, a novel multi-channel waveform agile radar testbed - ASTAP (Advanced Space-Time Adaptive Processing) with eight transmit channels and a single receive channel to form a co-located Multiple-Input Single-Output (MISO) radar is presented. Based on current configuration, the ASTAP radar system possesses agility for synthesizing and transmitting independent waveforms via each transmit channel simultaneously via multi-channel Arbitrary Waveform Generator (AWG). Hardware imperfections influence on digitally created waveforms including limited-bits DAC (Digital-to-Analog Converter) quantization, inter-channel time- and phase-skew (and/or jitter), non-linearities introduced by high-frequency devices (RF amplifiers and mixers etc) and antenna dispersion effects has been studied experimentally.

An end-to-end system-level digital calibration using Over-the-Air (OTA) channel measurements to minimize system hardware imperfections prior to transmission is proposed. Calibration accuracy for waveform transmit ambiguity functions, orthogonality in MISO transmissions, received signals separation and beamforming process for the synthesis of target azimuth distributions is examined and quantified. Front-end performance with different waveforms types for colored transmission and simultaneous MIMO is demonstrated and analysed. Extraction of the signals corresponding to each transmit channel from the composite received signal in a single receive channel exploiting waveforms orthogonality is studied experimentally.

**Index Terms**—Coded waveforms, front-end calibration, multi-channel radar demonstrator, MISO transmissions, multi-beam processing, multi-channel front-end, OTA measurement calibration, waveform agility.

## I. INTRODUCTION

Phased-array technology has been widely used in radar systems employing a focused beam to scan a larger area by successive beam steering. The benefit obtained is long range tracking of target with smaller Signal-to-Noise ratio (SNR) values, provided that the target direction is known a priori [1],[2]. Alternatively, wide-illumination beam can be employed to cover large angular sector and forming directive stacked beams on reception by means of Digital Beamforming (DBF). The spatial diversity obtained in this case corresponds to a final result which is equivalent to phased-array scanning in terms of energy [3],[4]. The low transmit-gain due to beam widening is compensated by a allowing a longer coherent processing interval (CPI) time, or simply, a longer time on target which directly corresponds to high Doppler resolution [2]. This is helpful in extraction of slow targets from clutter, short-range defence or collision avoidance when smaller reaction time is required.

Radar transmission strategies

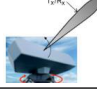
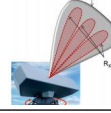
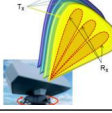
Transmission Beam	Narrow	Wide	Multiple
Reception beams	Narrow	Narrow	Narrow
Angular resolution	optimal	degraded	optimal
Time on target	limited	optimal	optimal
Space coverage	limited	enhanced	optimal
Beam illustration			

TABLE I: Comparison of different illumination strategies

In some application-specific situations, DBF can be extended to transmit multiple independent waveforms such that wide angular space can be illuminated and the back-scattered signals can be separated exploiting waveforms orthogonality on reception. In other words, the clutter being injected through the antenna sidelobes can be eliminated from the target echoes coming through the antenna mainlobe, as now these are "colored" by the transmission codes. The trade-off cost is the increased instantaneous signal bandwidth required for the number of coded beams [2]. Based on operational requirements, comparison among different beam strategies is presented in Table I.

Overview of demonstrators for simultaneous waveform transmission

	Tx/Rx Channels	Frequency	Bandwidth
BEEMER [5]	4/4	3.5 GHz	40 MHz
HYCAM [6],[7]	12/16	S-Band	500 MHz
MATE [8]	8/1	28.5 GHz	1 GHz
RIAS [9]	25/48	VHF	250 kHz
MMRS [10]	2/4	9.55 GHz	150 MHz
MISO RADAR [11]	4/1	16 GHz	–
ASTAP (this paper)	8/1	9.4 GHz	200 MHz

TABLE II: Comparison of various multi-channel radar testbeds

Comparing to the conventional radars exploiting multiple degrees of freedom on receive; MIMO radars allow to exploit similar benefits on transmit using multiple independent transmissions[12],[13],[14],[5],[15] and [16]. However, a few multi-channel radar testbeds are developed in [5],[6],[8],[9],[10],[11] to support simultaneous independent signal transmissions and are listed in Table II. In this paper, architecture and design of a novel multi-channel waveform

agile radar system demonstrator is described, its over-the-air calibration is presented and its performance is characterized. With only single receiver channel, decomposition of different transmitted orthogonal codes in the receiver is considered and impact of the transmit hardware on the transmitted waveform orthogonality is studied experimentally. The rest of the paper is organized as follows. Section II presents the system hardware architecture overview and the end-to-end system calibration is described in Section III. The calibration accuracy using range-angle ambiguity functions and MISO signal separation is presented in Section IV followed by conclusions in Section V.

## II. ASTAP RADAR SYSTEM

The ASTAP radar system consisting AWG, High frequency Box (RF amplifiers and mixers etc) and series-fed antenna patch array is shown in Figure 1. The developed system architecture supports eight transmit channels and single receive channel to mainly focus on the transmit beamforming.

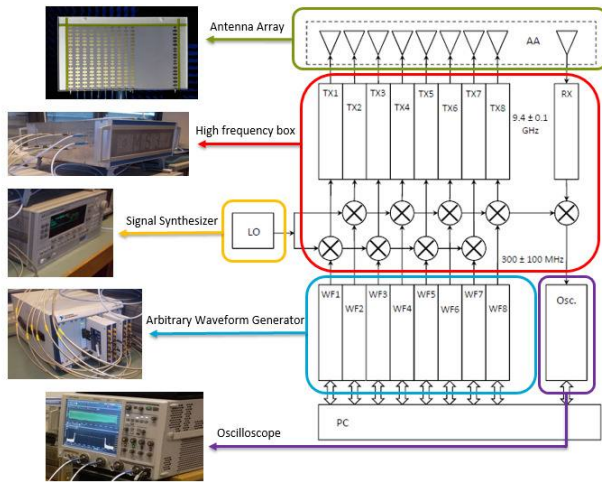


Fig. 1: ASTAP eight-transmit single-receive MISO radar testbed block diagram

The time-domain waveforms using MATLAB® are loaded into Arbitrary Waveform Generator via National Instruments Lab View® application interface. The digitally synthesised IF signals are then transformed to analog domain via four dual channel, 14-bit (8-bits usable in the ASTAP radar system configuration), AT-1212 Digital-to-Analog Converters (DACs) modules by Active technologies® [17]. The analog IF signals are up-converted by the multi-channel high-frequency box using a common local oscillator (LO) centered at 9.4 GHz to generate RF signals. The RF signal waveforms are radiated coherently via multiple series-fed patch antenna array arranged in regularly spaced Uniform Linear Array (ULA) to construct colored/MISO transmissions. The normalized radiation patterns of the ASTAP transceiver antenna array (H-plane and E-Plane cuts) are shown in Fig. 2.

On the receiver side, the composite back-scattered echo signals are captured by the single receive antenna and down-converted to IF stage. Currently, the IF signals are recorded directly using a Digital Storage Oscilloscope (DSO) for

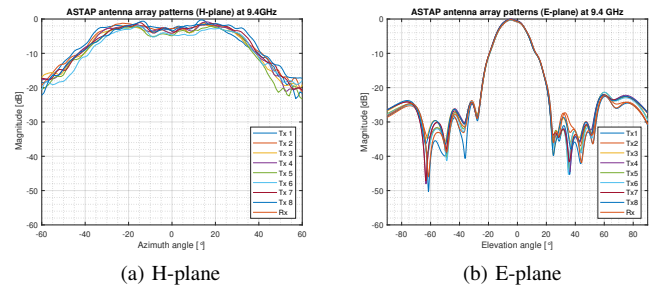


Fig. 2: ASTAP antenna array radiation patterns at 9.4GHz

preliminary measurement analysis. The RF specifications of the ASTAP radar system are presented in Table III.

ASTAP radar system specifications		
Parameters	Value	Unit
RF center frequency ( $f_0$ )	9.4	GHz
IF center frequency ( $f_c$ )	300	MHz
Single transmit channel gain	40	dB
Single transmit antenna gain	11.5	dBi
Output transmit power	+25.5	dBm
Receiver channel gain	40.4	dB
Receiver antenna gain	11.5	dBi
Receiver RF input (max.)	-25	dBm
Receiver sensitivity	-120	dBm
Receiver dynamic range	95	dB
Theoretical range resolution	0.75	m
Theoretical angular resolution	5.1	degrees

TABLE III: ASTAP radar system specifications

## III. SYSTEM CALIBRATION

The optimal calibration method using Over-the-Air (OTA) single channel measurements for ASTAP radar transmit signal pre-distortion is developed and is considered as the end-to-end calibration method whereas including the entire radar system along with microwave cabling assembly. As shown in Figure 3, these measurements in radiating-circuit setup have the added benefits of incorporating antenna effects and free-space channel as well as transmit/receive hardware channels asymmetries in signal amplitudes and phases.

It follows that the individual transmit-receive channel distortions in frequency-domain transfer-functions denoted by  $H(\omega)$  can be measured by collecting a reference LFM signal  $S_{lfm}(\omega)$  response through the ASTAP radar system as:

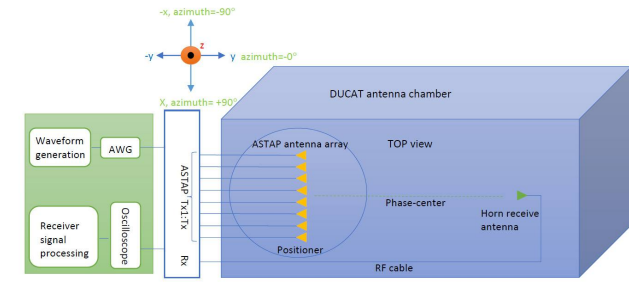
$$H(\omega) = \frac{Y_{lfm, distorted}(\omega)}{S_{lfm}(\omega)} \quad (1)$$

The measured transfer functions magnitude response  $|H(\omega)|$  and phase response  $\phi(H(\omega))$  of all channels are plotted in Figure 4a and 4b, respectively.

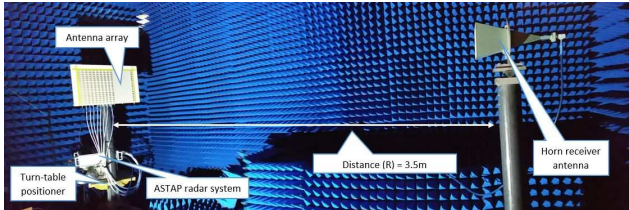
Using  $H(\omega)$ , the reference LFM signal can be pre-distorted as:

$$S_{lfm, predist}(\omega) = S_{lfm}(\omega) \times H^{-1}(\omega) \quad (2)$$

It is important to note that the inversion term  $H^{-1}(\omega)$  is very noise sensitive. So some regularization or pseudo-inversion is typically done. It can be computed similar

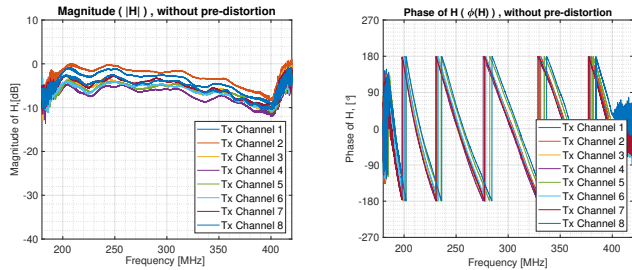


(a) Measurement setup geometry illustration

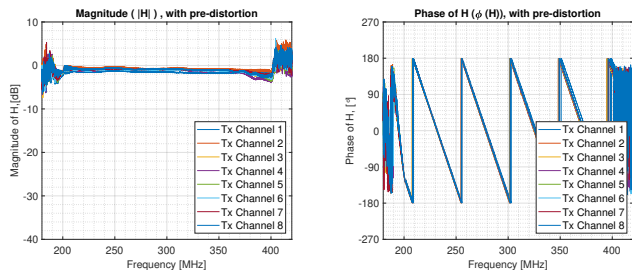


(b) ASTAP radar configured in anechoic chamber

Fig. 3: ASTAP radar system setup in anechoic chamber



(a) Magnitude response before calibration (b) Phase response before calibration



(c) Magnitude response after calibration (d) Phase response after calibration

Fig. 4: ASTAP radar system channels transfer function characterization

to as described in [18]. Afterwards, the predistorted signal frequency response ( $S_{lfm,predist}(\omega)$ ) is transformed to the time-domain signal ( $s_{lfm,predist}(t)$ ) and re-transmitted through the ASTAP radar system channel by channel. The corresponding received signal is collected through the horn antenna and recorded via the DSO to get the corrected signal response ( $Y_{lfm,corrected}(\omega)$ ):

$$Y_{lfm,corrected}(\omega) = S_{lfm,predist}(\omega) \times H(\omega) \quad (3)$$

Moreover, all the other signal waveforms ( $S_{WF}(\omega)$ ) are predistorted using  $H(\omega)$  as follows:

$$S_{WF,predist}(\omega) = S_{WF}(\omega) \times H^{-1}(\omega) \quad (4)$$

Finally, the corrected waveform output response ( $Y_{WF,corrected}(\omega)$ ) can be given similar to equation 3 as:

$$Y_{WF,corrected}(\omega) = S_{WF,predist}(\omega) \times H(\omega) \quad (5)$$

Using the equation 3, the transfer functions responses ( $H(\omega)$ ) for ASTAP radar system after calibration can be plotted in Figure 4c and 4d, respectively. From now on, the terms "calibration" and "predistortion" will be used interchangeably to indicate the system performance improvements in the different analyses.

#### IV. SYSTEM PERFORMANCE ANALYSIS

Once the ASTAP system is calibrated, it is subjected to waveforms transmission in the Delft University Chamber for Antenna Tests (DUCAT) [19], while configured in the radiation-circuit test (communication mode). The ASTAP system scans an angular space of  $\pm 60^\circ$  with  $1^\circ$  step while being mounted on the  $360^\circ$  positioner. At each phase-increment step, the measurement data are recorded for further signal analysis. The calibration accuracy is quantified considering the sidelobe level suppression in the range-angle plots using the Sidelobe Level (SLL) value. Constant Doppler effect within one pulse and periodic waveforms for eliminating long-range static clutter (e.g. mountains) are assumed. Table IV lists the simulation and measurement parameters for this section.

Simulation and Measurement parameters		
Parameters	Value	Unit
Pulse Width ( $T_p$ )	100	$\mu$ sec
Bandwidth (B)	200	MHz
RF center frequency ( $f_0$ )	9.4	GHz
IF center frequency ( $f_c$ )	300	MHz
Sampling frequency ( $f_s$ )	1.25	GS/s
No. of antenna elements	8	-
Inter-element distance(d)	$1.25 \times \lambda$	m
Azimuth scan range ( $\theta$ )	$\pm 60$	degree
Azimuth scan step	1	degree
No. of scan steps	121	-
Waveforms Used		
Single LFM	-	-
Circulating LFM	-	-
Delft Codes	CircLFM + Barker code-7	-
Hybrid Codes	CircLFM + Golay pair-8	-
Gold Codes	Code length ( $N_c$ ) = 2047	chip
Kasami Codes	Code length ( $N_c$ ) = 4095	chip

TABLE IV: Simulation and measurement parameters specifications

##### A. Spatial-spectral signal distribution

At first, the phased-array case with a single LFM transmission is considered as shown in Figure 5.

The uncalibrated measurement results contain quite high sidelobe level with main lobe gain fluctuation and grating lobes appearing in the visible region as shown in Figure 5a. The SLL is reduced significantly after calibration with near-constant mainbeam magnitude (Figure 5b). The azimuth and frequency response at center frequency and boresight are presented in Figure 5d and Figure 5c, respectively to



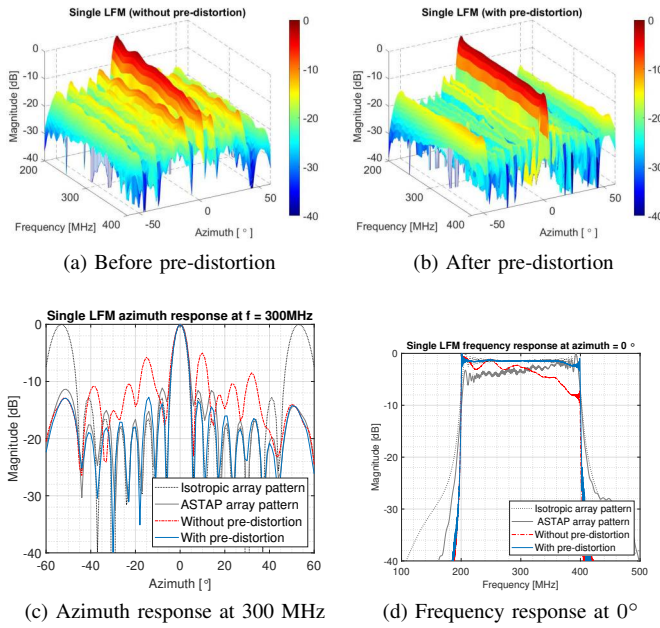


Fig. 5: Single LFM spatial-spectral signal distribution

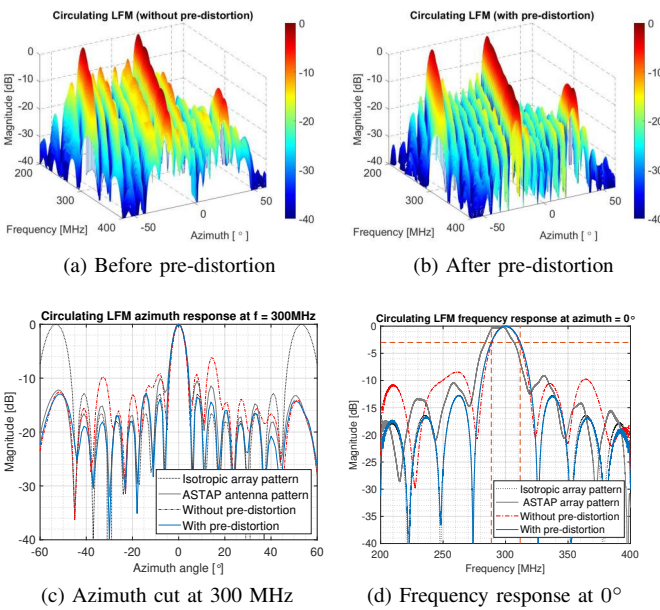


Fig. 6: Circulating LFM signal distribution (frequency vs azimuth) pre- and post-distortion

demonstrate the improvement of sidelobe level. The comparison between isotropic radiators, ASTAP antenna array only response, the complete system integration response with and without pre-distortion is done to illustrate calibration accuracy.

In the case of circulating LFM, the SLL is suppressed to around -13.5dB after pre-distortion as shown in Figure 6. The calibration also compensates the antenna pattern imperfections with an improvement of about 3dB in the SLL for the resulting scanning beam. Furthermore, the frequency response is plotted in Figure 6d. The 3dB mainlobe width corresponds to a frequency bandwidth of 25MHz (illustrated by two vertical orange dashed lines), such that the effective

range resolution is degraded by a factor of 8 ( $\frac{B}{N} = \frac{200M}{8} = 25\text{MHz}$ ); the characteristic trade-off using this waveform.

### B. Range-angle ambiguity function

As shown in Figure 7, each vertical-cut is a range profile ( $|\chi_0(\frac{c\tau}{2}, 0)|^2$ ) in the observed direction ( $\theta'$ ), while the beamforming has been done in the direction ( $\theta_0$ ). Each horizontal-cut is an observed direction ( $\theta'$ ) profile  $|\chi_0(0, \theta')|$ , while the beamforming has been done in the direction ( $\theta_0$ ).

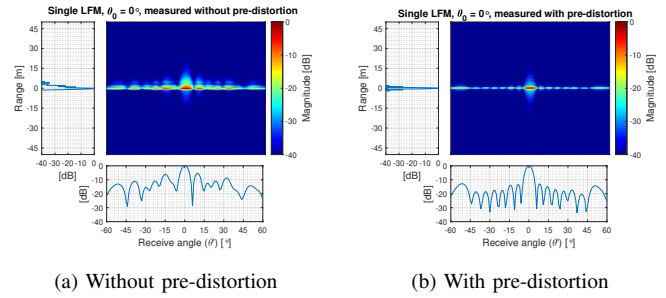


Fig. 7: Single LFM range-angle ambiguity function

The side-by-side comparative ambiguity function responses for rest of the considered waveforms with and without pre-distortion operation are processed and presented in the Figure 8. The range- and angle-domain SLL comparison between all the waveforms is presented in Table V. The SLL after calibration has improved significantly for almost all the waveforms.

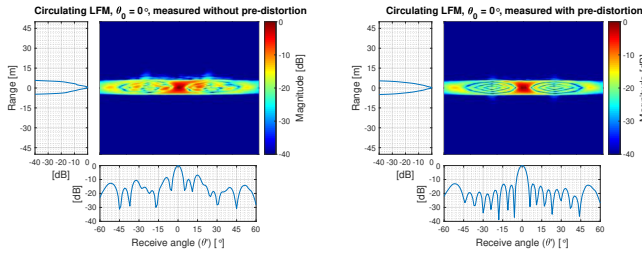
### C. MISO signal transmission and separation at receiver

To perform the antenna-specific signal separation and transmit beamforming, the Kasami coded signal waveforms are transmitted through the calibrated radar system in the communication mode (see Figure 3). In the first experiment, single code (code 1) is used to modulate the LFM signal and radiated through each transmit channel. Afterwards, all eight codes are transmitted through respective antenna sub-array elements, thus creating MISO illuminations on transmit.

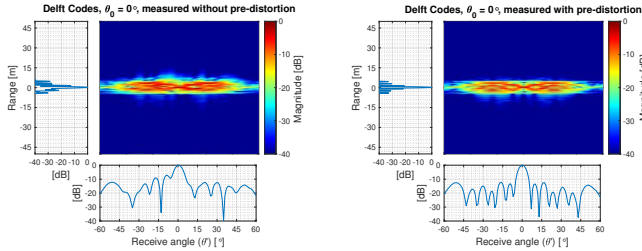
Matched filtering of the received composite signal is done with each of the transmitter-specific Kasami coded sequences [code 1, code 2, ..., code 8] which are used with the ASTAP radar system. Figure 9a shows that the matched filtering process results the phased-array case since the same waveform is transmitted through each antenna-element in first experiment. The correlation with rest of the codes also results similar patterns due to the code leakage in cross-correlation, and normalized peak magnitude of code 1 relative to other peaks indicates the orthogonality between the codes of about 33dB.

As for the second case, the transmitted signals are incoherent with each other and remain spread through the observed angular domain, thereby creating wide beams illumination as shown in Figure 9b. The gain fluctuations are present inherently in the elements embedded radiation patterns (see Figure 2).

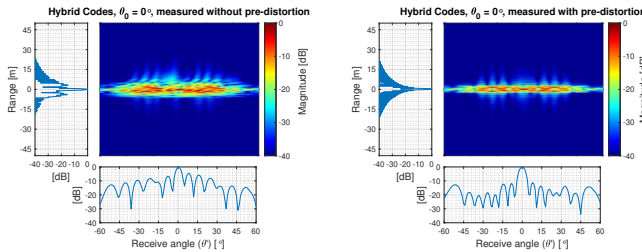
The second step in the received signal processing is the digital beamforming on transmit which is essentially a Fourier Transform (or Spatial filter, beamforming for direction). In principle, for each beamformed direction ( $\theta_0$ ) on transmit, one received direction ( $\theta'$ ) has to be examined



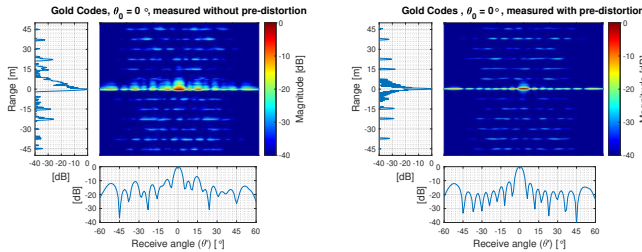
(a) Circulating LFM Without pre-distortion (b) Circulating LFM with pre-distortion



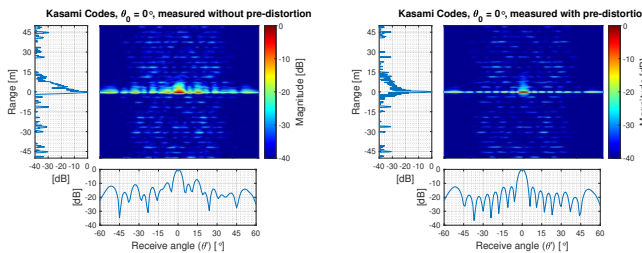
(c) Delft Codes without pre-distortion (d) Delft Codes with pre-distortion



(e) Hybrid Codes without pre-distortion (f) Hybrid Codes with pre-distortion



(g) Gold Codes Without pre-distortion (h) Gold Codes with pre-distortion

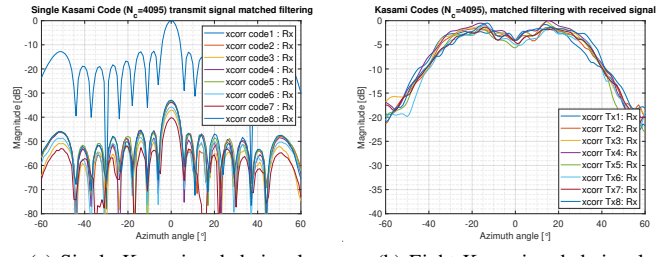


(i) Kasami Codes without pre-distortion (j) Kasami Codes with pre-distortion

Fig. 8: Range-angle ambiguity function responses

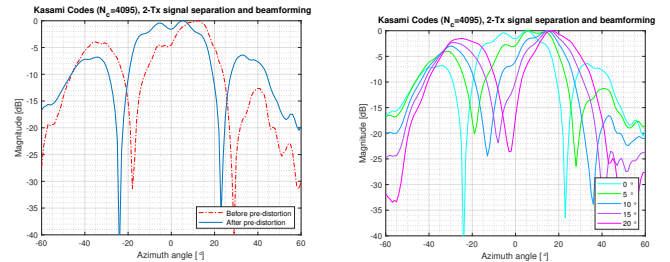
[20]. If there are more than one receive channel to create MIMO configuration, the beamforming on receive should be done as additional step.

The beamforming results considering uncalibrated and calibrated system responses are illustrated in Figure 10. The beamforming process before pre-distortion is spoiled

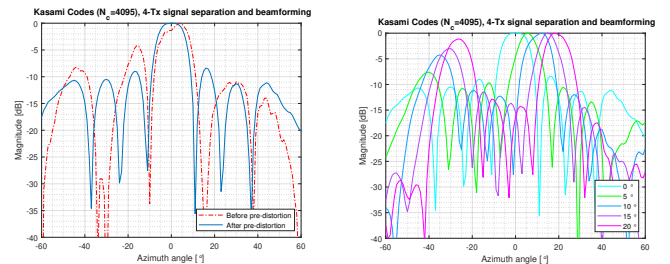


(a) Single Kasami coded signal (b) Eight Kasami coded signal

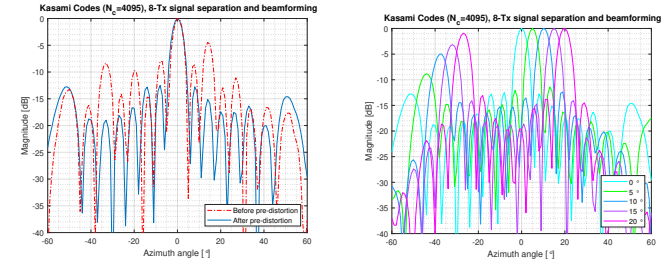
Fig. 9: Kasami Codes matched filtering with measured received signal



(a) Two-elements beamforming (b) Two-elements beam scanning



(c) Four-elements beamforming (d) Four-elements beam scanning



(e) Eight-elements beamforming (f) Eight-elements beam scanning

Fig. 10: Calibration impact on transmit signal beamforming and angular scanning

significantly by higher sidelobes along with erroneous beam orientations in all three cases. However, the after-calibration beamforming accurately points to the correct direction and the angular sidelobes are suppressed reasonably. The grating lobes also appear in the visible angular range for large scanning angles which means that the angular ambiguity can cause false alarms.

## V. CONCLUSION

In this paper, the novel investigation of the impact of system imperfections on the orthogonality of the waveforms in a MIMO radar is presented using ASTAP radar system

Waveforms	Range-domain SLL (dB)			Angle-domain SLL (dB)		
	Simulations	Measurements		Simulations	Measurements	
	ASTAP array	Without calibration	With calibration	ASTAP array	Without calibration	With calibration
Single LFM	-12.67	-13.90	-13.95	-10.34	-5.40	-12.87
Circulating LFM	-30.61	-52.81	-79.09	-8.86	-6.78	-13.13
Delft codes	-10.25	-13.03	-20.8	-8.60	-7.20	-13.25
Hybrid codes	-12.51	-14.90	-13.76	-13.37	-4.55	-11.26
Gold codes	-23.98	-7.72	-15.16	-9.44	-7.10	-10.88
Kasami codes	-28.29	-7.46	-16.32	-9.07	-7.45	-12.58

TABLE V: Range and angular sidelobe level comparison for different waveforms

characterization. A novel calibration scheme for compensating system imperfections on transmit-side by pre-distorting the signal waveforms using over-the-air (OTA) channel measurements is developed. Different coded waveforms are transmitted through the ASTAP radar system to observe the calibration accuracy using waveform spatial-spectral signal distribution and range-angle ambiguity function plots. Furthermore, up to  $12^\circ$  beam pointing error in the uncalibrated beamforming process is corrected by the calibration scheme. The obtained results show a good agreement with the simulated results using pre-defined radar parameters.

#### ACKNOWLEDGMENT

The authors would like to acknowledge ir. Peter Swart for the development of the high-frequency box, ir. Dinh Tran for antenna array design and development. The acknowledgement is extended further to Prof. dr. ir. Francois Le Chevalier for elaborating physical sense of colored transmission concepts and Max Ian Schope for frequent discussions.

#### REFERENCES

- [1] D. R. Fuhrmann and G. San Antonio, "Transmit beamforming for MIMO radar systems using signal cross-correlation," *IEEE Transactions on Aerospace and Electronic Systems*, pp. 171–186, January 2008.
- [2] F. Le Chevalier, "Future concepts for electromagnetic detection: from space-time-frequency resources management to wideband radars," *IEEE Aerospace and Electronic Systems Magazine*, pp. 9–17, October 1999.
- [3] B. D. Van Veen and K. M. Buckley, "Beamforming: a versatile approach to spatial filtering," *IEEE ASSP Magazine*, pp. 4–24, April 1988.
- [4] T. Jeffrey, "Phased-array radar design - Application of radar fundamentals," 2009.
- [5] T. C. Mealey and A. J. Duly, "BEEMER: A firmware-tuned, software-defined MIMO radar testbed," in *2016 IEEE International Symposium on Phased Array Systems and Technology (PAST)*, October 2016, pp. 1–6.
- [6] P. Brouard, L. Constancias, A. Brun, S. Attia, J. Peyret, and P. Dreuillet, "Hycam: A new S-band surface radar testbed," in *IET International Radar Conference 2013*, April 2013, pp. 1–4.
- [7] M. Cattenoz and P. Brouard, "An experimental demonstration of a posteriori digital calibration of MIMO radar system," in *2014 International Radar Conference*, October 2014, pp. 1–5.
- [8] K. Buisman and T. Eriksson, "Designing and characterizing MATE, the Chalmers mm-wave MIMO testbed," in *12th European Conference on Antennas and Propagation (EuCAP 2018)*, April 2018, pp. 1–5.
- [9] Y. B. J. Dorey and F. Christophe, "Le projet RIAS, une approche nouvelle du radar de surveillance aérienne," in *Colloque International sur le radar, Versailles, France, 1984*.
- [10] T. Rommel, A. Patyuchenko, P. Laskowski, M. Younis, and G. Krieger, "Development of a MIMO radar system demonstrator - Calibration and demonstration of first results," in *2012 13th International Radar Symposium*, May 2012, pp. 113–118.
- [11] J. P. Stralka, R. M. Thompson, J. Scanlan, and A. Jones, "Miso radar beamforming demonstration," in *2011 IEEE RadarCon (RADAR)*, May 2011, pp. 889–894.
- [12] M. S. Davis, G. A. Showman, and A. D. Lanterman, "Coherent MIMO radar: The phased array and orthogonal waveforms," *IEEE Aerospace and Electronic Systems Magazine*, pp. 76–91, August 2014.
- [13] D. Cohen, Y. C. Eldar, and A. M. Haimovich, "SUM-MeR: Sub-Nyquist MIMO radar," *IEEE Transactions on Signal Processing*, pp. 4315–4330, August 2018.
- [14] S. D. Blunt and E. L. Mokole, "Overview of radar waveform diversity," *IEEE Aerospace and Electronic Systems Magazine*, pp. 2–42, November 2016.
- [15] U. K. Majumder, M. R. Bell, and M. Rangaswamy, "A novel approach for designing diversity radar waveforms that are orthogonal on both transmit and receive," in *2013 IEEE Radar Conference (RadarCon13)*, April 2013, pp. 1–6.
- [16] H. Sun, F. Brigui, and M. Lesturgie, "Analysis and comparison of MIMO radar waveforms," in *2014 International Radar Conference*, October 2014, pp. 1–6.
- [17] "Active Technologies AT-1212, high speed signal generator adapter module for NI FlexRIO."
- [18] T. G. Savelyev and A. G. Yarovoy, "Fast imaging by 3-D deconvolution in short-range UWB radar for concealed weapon detection," in *2012 9th European Radar Conference*, 2012, pp. 26–29.
- [19] "DUCAT, The Delft University Chamber for Antenna Tests," <http://radar.ewi.tudelft.nl/Facilities/ducat.php>.
- [20] F. Le Chevalier, *Wideband Wide Beam Motion Sensing*. CRC Press, November 2016, ch. 12, pp. 417–458.